# Measurements of the polarization parameter in $K^+p$ elastic scattering at low energies

B. R. Lovett,* V. W. Hughes, M. Mishina,† and M. Zeller
*Physics Department, Yale University, New Haven, Connecticut 06520*

D. M. Lazarus
*Brookhaven National Laboratory, Upton, New York 11973*

I. Nakano‡
*Physics Department, Kyoto University, Kyoto, Japan*
(Received 10 September 1980)

Results of measurements of the polarization parameter in $K^+p$ elastic scattering at 650, 700, 845, and 940 MeV/$c$ are presented. Details of the measurements are described and results are compared with previous measurements and partial-wave parametrizations of the data. The implication of the existence of $Z^*$ resonances in light of these results is discussed.

## INTRODUCTION

The discrepancy between experimental observations of structure in $K^+N$ total cross sections[1] and theoretical predictions of the absence of structure in strangeness +1 baryon resonances[2] has motivated extensive studies of $K^+N$ interactions in recent years. In particular, $K^+p$ scattering has produced a great deal of information on the possible existence of pure $I = 1$ resonant states. These data also constrain the $I = 0$ analyses which are obtained primarily from $K^+n$ data which are a superposition of $I = 0$ and $I = 1$ amplitudes. A large data base has been gathered which contains results of total- and differential-cross-section measurements at laboratory beam momenta of 160 MeV/$c$ and above,[1,3-5] and polarization-parameter $P$ measurements at momenta of 870 MeV/$c$ and above.[5,6] Analyses of these data have suggested the existence of exotic $Z^*$ resonances but, even with the large amount of data, such states have not been conclusively confirmed.

Prior to the experiment described in this article, predictions of polarization parameters at momenta below 870 MeV/$c$, from analyses which both included and excluded resonance solutions, had been made by several authors.[4,5,7-9] To test these predictions and to broaden the data base for future work, we have extended the measurements of $P$ from 870 MeV/$c$ down to 650 MeV/$c$. In particular, we have measured $P$ at beam momenta of 650, 700, 845, and 940 MeV/$c$ which correspond to center-of-mass energies of 1630, 1653, 1720, and 1765 MeV, respectively. Our apparatus covered a broad angular range ($-0.8 < \cos\theta_{\text{c.m.}} < 0.8$), and utilized the intense low-energy separated beam (LESB I) at the Brookhaven National Laboratory Alternating Gradient Synchrotron.

In this paper we describe the detection apparatus which was also used in our previously reported measurements of $K^-p$ elastic-scattering polarizations,[10] we give a detailed account of the data reduction and analysis, and finally, we discuss our results in comparison with several predicitions.

## APPARATUS

A schematic drawing of the apparatus is shown in Fig. 1. As mentioned above, the LESB I, which transmitted a momentum band of approximately $\pm 2.0\%$, provided the partially separated beam of $K^+$ mesons. Fluxes ranged from $3\times10^3$ to $1.2\times10^4$ per $10^{12}$ protons incident on the production target, with $K^+/\pi^+$ ratios ranging between 0.26 and 0.43. These ratios were increased to greater than 33 by use of a liquid-cell differential Čerenkov counter $\check{C}_B$, which gave both positive identification of the kaons and a veto signal for pions. Determination of the incident-particle trajectories was made in the horizontal plane by proportional wire chambers $WBH_1$ and $WBH_2$, and in the vertical plane by chamber $WBV$; the beam had a horizontal convergence of $\sim\pm 100$ mrad and a vertical convergence $\simeq \pm 10$ mrad.

It was required that the apparatus detect the two final-state particles over a wide angular range with sufficient angular resolution to enhance the elastic signal with respect to background; the background is mainly quasielastic scattering of the kaons by bound protons in the target material. The detector system was cylindrically disposed about a vertical line through the magnet center, and was separated into beam-left and beam-right sides with horizontal angular acceptances of 118° and 109°, respectively.

Determination of the horizontal component of final-state particle trajectories was made with the cylindrical proportional chambers $W\theta_L$ and $W\theta_R$, and scintillation counters $\theta_L$ and $\theta_R$ for the

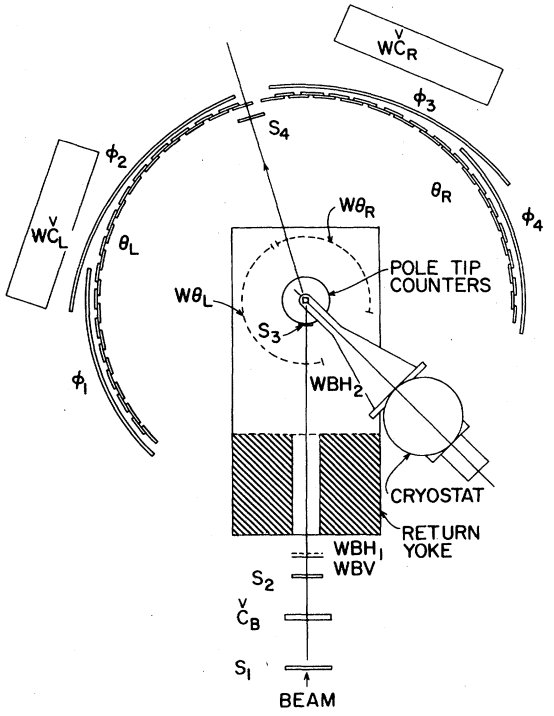


FIG. 1. Plan view of the detection apparatus. The polarized proton target is at the center of the cylindrical proportional-wire-chamber system formed by $W\theta_R$, $W\theta_L$, and $WBH_2$. $S_1$–$S_3$ are scintillation counters used in the trigger and $S_4$ is a veto counter which rejects triggers with unscattered particles. $\theta_L$ and $\theta_R$ are scintillation-counter hodoscopes made up of overlapping counters. $\phi_1$-$\phi_2$ are banks of ten scintillation counters each, defining the azimuthal angle of scattering.

left and right sides of the apparatus, respectively. The sense wires of the proportional chambers were located on a radius of 29.3 cm with a wire spacing of 2 mm, while the scintillation counters were at a radius of 76.2 cm and were 7.6 cm wide with a 2.5 cm overlap with their two neighbors. Note was taken of trajectories that passed through one or two counters and thus the angular resolution of these outer detectors was 33 mrad.

For determination of the vertical component of particle trajectories, four banks of 10 scintillation counters each, $\phi_1 - \phi_4$, were placed at a radius of 81.3 cm from the magnet center. The counters in banks $\phi_2$ and $\phi_3$ were tapered into an "orange peel" shape so that each counter had a height approximately equal to $(5.1 \times \sin\theta)$ cm, where $\theta$ is the laboratory polar angle of scattering of the final-state kaon; the trajectory of an unscattered beam particle defined the $z$ axis. Thus the detector subtended an approximately constant azimuthal scattering angle for all accepted polar angles.

Figure 2 is a plot of the angle of the outgoing proton vs that of the outgoing kaon for elastic scattering at 650 MeV/$c$. There is a plot for both $K^+$ scattering to the right side of the apparatus and one for the $K^+$ scattering to the left, with the numbers on the plots being the $\cos\theta_{c.m.}$ scattering angles for selected points. On this graph, one can see the limits of the $\theta$ counters and the overlap and taper regions for the $\phi$ counters. Note that near $\cos\theta_{c.m.} = 0$ for both $K^+$ left and $K^+$ right, the two plots overlap, i.e., determination of $K^+$ left or $K^+$ right cannot be made from particle trajectories alone. This determination must be made by a measurement of the velocities of the respective particles, to which end a combination of information from water-filled Čerenkov counters, $W\check{C}_L$ and $W\check{C}_R$ in Fig. 1, and particle time of flight to the $\phi$ counters was used. The method of particle identification will be described in greater detail below.

In addition to the detectors which determined initial- and final-state particle trajectories, scintillation counters $S_1$–$S_3$ were used to trigger the system on an incoming beam particle, with a veto by $S_4$ to establish that the beam particle did not exit the target without being scattered. Counter $S_3$, 1.3 cm high by 2.0 cm wide, established that the particle had passed through the polarized target material and served as the time-of-flight reference for the $\phi$ counters. Covering the pole tips of the target magnet were a pair of counters, each of which was a "sandwich" of 0.32 cm of tungsten between two 0.32-cm-thick pieces of scintillation material, designed to veto the trigger if charged particles or photons exited the target vertically. These counters were designated $PT_1$ and $PT_2$.

The trigger for the system was thus satisfied by a coincidence between the counters $S_1$–$S_3$, an anti-

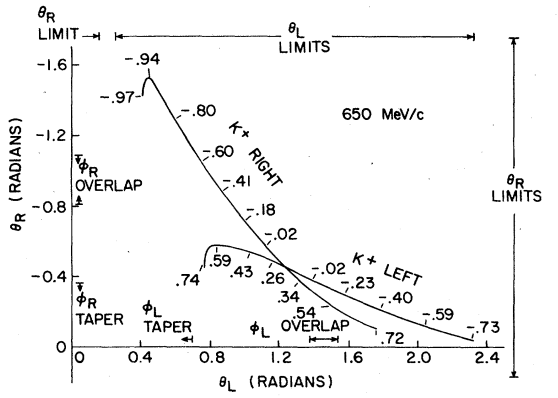


FIG. 2. Correlation plot of scattering angles of the final-state particles in the laboratory. The numbers on the curves are values of $\cos\theta_{c.m.}$. Also shown are the limits of the $\theta_L$ and $\theta_R$ counters and the $\phi$ counters.

coincidence with the counters $S_4$ and $PT_1$, and $PT_2$, and a positive identification of an incident kaon by $\check{C}_B$. In addition, a rough coplanarity requirement on the trajectories of the final-state particles with that of the beam was established by a matrix coincidence between the left and right banks of $\phi$ counters. This requirement necessarily satisfied the condition that there be two particles in the final state, one on either side of the apparatus.

The trigger having been satisfied, the status of each detector in the system was read into a Digital Equipment Corporation PDP15 computer. This information included all proportional chamber wires, all scintillation counters, the pulse heights from the Čerenkov counters, time-of-flight information for the $\phi$ counters, and various scalers used to monitor the system and later used to normalize the numbers of events gathered. The computer packed the data into words which contained the identity of those channels, wire or counter, which participated in the event. It then wrote this information, along with pulse height, time of flight, and scaler data, on magnetic tape. The computer also was used to monitor the operation of the apparatus by constructing frequency distributions of detector elements and pulse-height and time-of-flight spectra.

### Polarized proton target

Maintained at ~0.55° K by a $^3$He-$^4$He refrigerator system, the polarized proton target material was situated in the gap of a "*C*" magnet which produced a magnetic field of 2.5 T. The target material, butanol doped with a free radical of porphyrexide and shaped into 1.5-mm spheres, filled a cavity 2.0 cm horizontally transverse to, 2.3 cm along, and 2.1 cm vertically transverse to the incident beam. The target was polarized by dynamic nuclear orientation with the polarization being measured by a fast-frequency-sweep NMR system. The absolute magnitude of the polarization, approximately 55% throughout the experiment, was determined by comparing the unenhanced thermal equilibrium signal with the enhanced signals. The uncertainty in the magnitude of polarization of the target was estimated to be ±5%.

### Data analysis

The Brookhaven On-Line Data Facility computers, Digital Equipment Corporation PDP10's, were used in the first stage of the data analysis. Since the raw data tapes contained many events that could be easily rejected as not being elastic-scattering candidates, only those events that satisfied the following requirements were retained for further processing: (1) One and only one reconstructable beam track; (2) horizontal position and angle of the beam trajectory being within predefined limits; (3) one and only one scattered-particle cluster within each of the cylindrical proportional chambers on either side of the apparatus; (4) one and only one scattered particle in each $\theta$ counter bank, $\theta_L$ and $\theta_R$: and (5) one and only one scattered particle in the $\phi_L$ counters, $\phi_1$ and $\phi_2$, and the $\phi_R$ counters, $\phi_3$ and $\phi_4$.

Those events which satisfied the above requirements were recorded on another tape, the condensed data tape, in a format which included the information from the raw data tapes as well as the horizontal transverse position and angle of the beam trajectory at the target as determined from the beam proportional chambers. In addition to recording the desired events, this phase of analysis further monitored the operation of the detector by maintaining a record of numbers of events failing the various cuts, and produced histograms of beam distributions.

The second stage of analysis involved comparing the observed hit points in the various detectors with corresponding calculated points resulting from a $\chi^2$ minimization to an elastic-scattering hypothesis. The Brookhaven Central Scientific Computing Facility computers were used for this purpose.

We describe in the Appendix the details of the procedures for event reconstruction and note here that for each event we determined and recorded on a summary tape the following: a value of $\chi^2$ for the fit to an elastic-scattering hypothesis; an estimator of the coplanarity of incoming and outgoing particle trajectores, $\Delta\phi = (\phi_K - \phi_\pi - 180°)/(\delta\phi_K{}^2 + \delta\phi_P{}^2)^{1/2}$, where $\delta\phi_K$ and $\delta\phi_P$ are the errors on the measured $\phi_K$ and $\phi_P$, respectively; a calculated longitudinal interaction point, $z_B$; and a value of $\cos\theta_{\text{c.m.}}$ resulting from the kinematic fit. For all of these quantities, results for both $K^+$-left and $K^+$-right hypotheses were retained. In addition, we recorded the horizontal transverse position and angle of the beam trajectory at the target center and the time-of-flight and pulse-height information. A right-handed coordinate system was used to represent the position of the interaction point with respect to the center of the system, i.e., $z_B$ is measured along the beam, $y_B$ is in the vertical direction, and $x_B$ is in the horizontal direction perpendicular to the beam.

The final processing which determined the numbers of elastic events in our sample involved sorting the summary tape for those events which had both small $\chi^2$ and small $\Delta\phi$ with values of $z_B$ within the target region. Referring to Fig. 2, we see that over most of the kinematic range of the experiment, the $K^+$-left and $K^+$-right hypotheses are spatially well separated. In the regions

where this separation is large, the two hypotheses have quite different values of $\chi^2$. This allowed us to choose one hypothesis over the other by requiring a $\chi^2$ difference of at least 3 and considering the hypothesis with the lower $\chi^2$ as the valid one.

Once chosen, the events with acceptable values of $x_B$ and $z_B$ could be arrayed in a plot of $\chi^2$ vs $\Delta\phi$. Distributions of numbers of events as functions of $\chi^2$ and $\Delta\phi$ are shown in Fig. 3. As a result of Monte Carlo calculations and distributions such as those in Fig. 3, the $\chi^2$ vs $\Delta\phi$ plot was divided into regions as shown in Fig. 4. Only events in the "signal" region were used in the evaluation of the polarization parameter, with the number of background events being estimated by an extrapolation of the "wings" through this area. In the range $-0.05 < \cos\theta_{\text{c.m.}} < 0.356$ for either hypothesis, which was termed the confusion region, kinematic separation of events was not sufficient and it was necessary to include information about the final-state particle velocities in the analysis. For the lower two momentum points, this information was derived from measurements of the

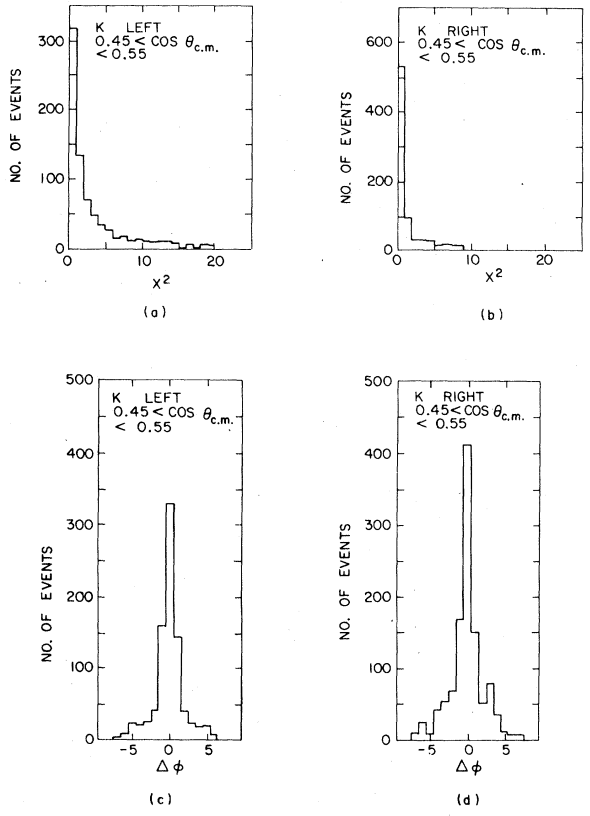


FIG. 3. (a) and (b) Distributions of numbers of events vs $\chi^2$ for $|\Delta\phi| < 2.5$. (c) and (d) Distributions of numbers of events vs $\Delta\phi$ for $\chi^2 < 5$.

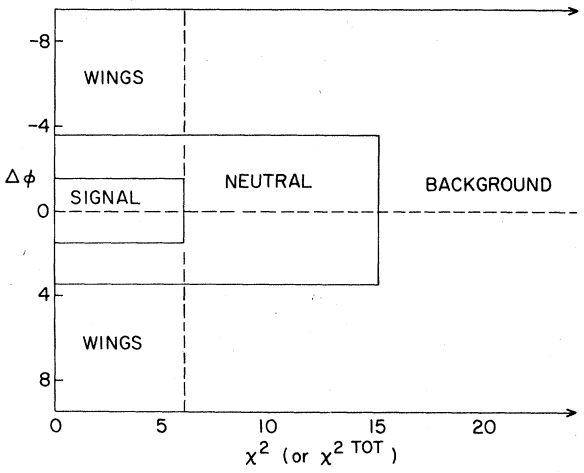


FIG. 4. Definition of regions in $\chi^2$-$\Delta\phi$ space.

time differences between the pulse in the $S_3$ counter and those in the two $\phi$ counters participating in the event. These are nominally the times of flight of the final-state particles from the target to the periphery of the apparatus, a distance of approximately 1 m.

Once the kinematic reconstruction was complete, the times of flight for each particle for each hypothesis could be calculated and recorded on the summary tape: $T_K^L$, $T_p^L$, $T_K^R$, $T_p^R$ for kaons and protons for the $K^+$-left and $K^+$-right hypotheses, respectively. Also recorded were the measured times to the left and right sides of the apparatus, $T_M^L$ and $T_M^R$. A $\chi^2$ value relating to the time measurements could then be formed for the left and right hypotheses, i.e.,

$$\chi_L^{2(T)} = \left(\frac{T_M^L - T_K^L}{\sigma_K}\right)^2 + \left(\frac{T_M^R - T_p^L}{\sigma_p}\right)^2 \tag{1a}$$

and

$$\chi_R^{2(T)} = \left(\frac{T_M^R - T_K^R}{\sigma_K}\right)^2 + \left(\frac{T_M^L - T_p^R}{\sigma_p}\right)^2, \tag{1b}$$

where $\sigma_K$ and $\sigma_p$ are the time-measurement uncertainties for the kaon and proton, 0.94 and 1.13 ns, respectively. This $\chi^2$ was then added to the respective $\chi^2$ from kinematics yielding a total value of $\chi^2$ for each hypothesis,

$$\chi_L^{2\,\text{tot}} = \chi_L^2 + \chi_L^{2(T)} \tag{2a}$$

and

$$\chi_R^{2\,\text{tot}} = \chi_R^2 + \chi_R^{2(T)}. \tag{2b}$$

As the events moved into the confusion region, the angular components of $\chi^{2\,\text{tot}}$ became equal for the two hypotheses, but the time components were different, thus permitting the correct hypothesis to be chosen.

For the higher-momentum points, 865 and 940 MeV/$c$, the time-of-flight difference between kaons and protons was too small to permit reliable resolution of the kinematic ambiguity. At these points, however, the kaons in the confusion region had velocities greater than those needed to produce Čerenkov light in water while the proton velocities were below this threshold. Thus, the water-filled Čerenkov counters, $W\check{C}_L$ and $W\check{C}_R$ in Fig. 1, were employed to resolve the ambiguity.

Due to geometrical effects and interactions with the water in the counters, not all kaons gave sufficient light to be unambiguously identified. Proper discrimination levels were determined both by placing the counters directly in the beam for calibration purposes and by considering pulse amplitudes for events where the particles passed through the counters but were kinematically identifiable. In the confusion region, the requirement that an event be correctly identified, and thus included in the final data sample, was that one particle be above this discrimination level and the other be below. The efficiency for meeting this requirement was approximately 30% and the probability of misidentification, as determined by the above mentioned study, was approximately 3%. The inefficiencies do not affect the polarization measurements beyond reducing the number of events, and a small correction for misidentification was made in the final analysis.

Once the number of elastic events was determined for each $\cos\theta_{\text{c.m.}}$ bin, the asymmetries in these numbers were calculated for the different orientations of the target polarization:

$$A_L(\cos\theta_{\text{c.m.}}) = \frac{N_L^U(\cos\theta_{\text{c.m.}})/K^U - N_L^D(\cos\theta_{\text{c.m.}})/K^D}{S_L^U(\cos\theta_{\text{c.m.}})/K^U + S_L^D(\cos\theta_{\text{c.m.}})/K^D} , \tag{3}$$

where $N_L^D, N_L^U$ refer to the total number of events observed for polarization antiparallel and parallel to the normal to the scattering plane for $K^+$- left events, $S_L^D, S_L^U$ are the numbers of signal events, and $K^D$ and $K^U$ are the effective numbers of kaons incident on the target for the two polarization orientations. The asymmetries for $K^+$-right events were calculated in the same manner; however, the order of terms in the numerator was reversed to maintain consistency with the Basel convention.[11] The total asymmetry, $A(\cos\theta_{\text{c.m.}})$ was then expressed as the weighted average of $A_L$ and $A_R$.

The determination of numbers of events has been discussed above. The numbers of incident kaons were scaled by the beam telescope counters in coincidence with $\check{C}_B$, and were corrected for the following effects: (1) Pion contamination as determined by accidental coincidences between the beam telescope and $C_B$, typically 3%; (2) accidental rejection of the incident beam by the veto counter $S_4$, typically 20%; (3) inefficiencies in beam-track reconstruction as determined by studies of beam tracks without requiring interactions, typically 15%; and (4) fraction of the incident beam missing the target or with incident angles outside of acceptable limits as determined by the above mentioned beam studies, typically 10%.

The final numbers of effective incident kaons and data events are listed in Table I.

The final polarizations for each $\cos\theta_{\text{c.m.}}$ bin were calculated according to the formula

$$P(\cos\theta_{\text{c.m.}}) = \frac{2A(\cos\theta_{\text{c.m.}})}{P_T^U + P_T^D - (P_T^U - P_T^D)A(\cos\theta_{\text{c.m.}})} , \tag{4}$$

where $P_T^U$ and $P_T^D$ were average target polarization values for target spin orientation up and down, respectively, with the average taken over all the data in the momentum point. This formulation of polarization parameter derived from measured asymmetries correctly compensates for any difference in the magnitudes of the target polarizations for the different spin orientations. A calculation of polarization was made for both $K^+$-left and $K^+$-right data with the weighted average yielding the final results.

Since the apparatus was approximately symmetric about the beam line, similar numbers of $K^+$-left and $K^+$-right events were gathered. Independent measurements were thus made of $P$ from these two classes of events and showed no systematic deviation from being equal. Also, the asymmetry of events with large values of $\chi^2$ or large deviations from coplanarity was measured and found to be statistically consistent with zero. These checks allow us to assign a systematic error of less than ±0.03 on the values of $P$ due to possible time variations in detector efficiency or incorrect beam normalization.

## RESULTS AND CONCLUSIONS

The final results for the polarization parameters are listed in Table II and shown in Fig. 5. The

TABLE I. Summary of beams and data.

| Momentum (MeV/$c$) | $K^+/10^{12}$ protons | $K^+/\pi^+$ | Total $K^+$ [a] | Total elastic events |
|---|---|---|---|---|
| 650 | $3.1\times10^3$ | 0.26 | $11.3\times10^7$ | 8 400 |
| 700 | $4.3\times10^3$ | 0.37 | $14.2\times10^7$ | 13 400 |
| 845 | $12.5\times10^3$ | 0.43 | $29.0\times10^7$ | 23 900 |
| 940 | $8.9\times10^3$ | 0.40 | $20.8\times10^7$ | 16 400 |

[a] Effective numbers of incident $K^+$ as described in the text.

TABLE II. Polarization results.

| $\cos\theta_{c.m.}$ | $P$ 650 MeV/$c$ ($\sqrt{s}$ =1630 MeV) | $P$ 700 MeV/$c$ ($\sqrt{s}$ =1653 MeV) | $P$ 845 MeV/$c$ ($\sqrt{s}$ =1720 MeV) | $P$ 940 MeV/$c$ ($\sqrt{s}$ =1765 MeV) |
|---|---|---|---|---|
| −0.8 | 0.134 ± 0.163 | 0.042 ± 0.139 | 0.141 ± 0.089 | |
| −0.7 | 0.266 ± 0.082 | 0.225 ± 0.066 | 0.199 ± 0.045 | 0.177 ± 0.060 |
| −0.6 | 0.238 ± 0.075 | 0.295 ± 0.064 | 0.305 ± 0.045 | 0.232 ± 0.054 |
| −0.5 | 0.355 ± 0.077 | 0.170 ± 0.061 | 0.319 ± 0.043 | 0.335 ± 0.053 |
| −0.4 | 0.343 ± 0.073 | 0.350 ± 0.058 | 0.262 ± 0.044 | 0.284 ± 0.053 |
| −0.3 | 0.319 ± 0.077 | 0.319 ± 0.059 | 0.397 ± 0.048 | 0.399 ± 0.056 |
| −0.2 | 0.408 ± 0.069 | 0.356 ± 0.057 | 0.331 ± 0.048 | 0.408 ± 0.052 |
| −0.1 | 0.185 ± 0.068 | 0.304 ± 0.059 | 0.366 ± 0.093 | 0.442 ± 0.081 |
| 0.0 | 0.355 ± 0.103 | 0.343 ± 0.080 | 0.474 ± 0.272 | 0.512 ± 0.156 |
| 0.1 | 0.436 ± 0.138 | 0.427 ± 0.131 | 0.475 ± 0.229 | 0.524 ± 0.154 |
| 0.2 | 0.367 ± 0.131 | 0.392 ± 0.150 | 0.343 ± 0.200 | 0.698 ± 0.143 |
| 0.3 | 0.288 ± 0.105 | 0.326 ± 0.106 | 0.627 ± 0.172 | 0.739 ± 0.222 |
| 0.4 | 0.405 ± 0.079 | 0.346 ± 0.067 | 0.454 ± 0.096 | 0.570 ± 0.094 |
| 0.5 | 0.377 ± 0.070 | 0.375 ± 0.058 | 0.515 ± 0.057 | 0.598 ± 0.062 |
| 0.6 | 0.508 ± 0.143 | 0.386 ± 0.060 | 0.575 ± 0.047 | 0.598 ± 0.047 |
| 0.7 | 0.474 ± 0.186 | 0.345 ± 0.078 | 0.449 ± 0.040 | 0.635 ± 0.045 |
| 0.8 | | | | 0.556 ± 0.061 |

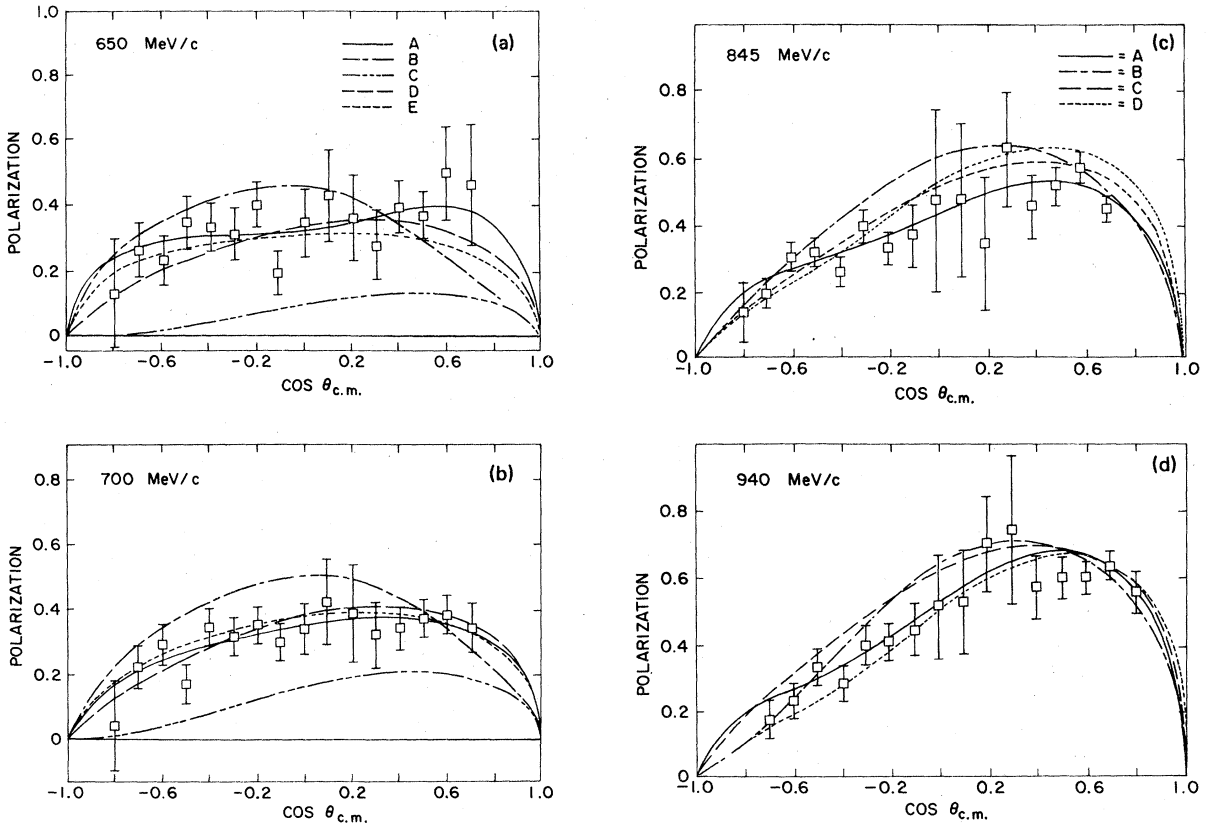


FIG. 5. Polarization parameter vs $\cos\theta_{c.m.}$ for various beam momenta. Curve A is the Legendre-polynomial fit described in text; B is from the energy-dependent partial-wave analysis of Ref. 4 which shows no $Z^*$ resonance; C and D result from the $K$-matrix analyses of Ref. 8 and 9, respectively, which have $Z^*$ resonances; E is obtained from a duality-diagram analysis using $\pi^+P$ background partial waves as input.

quoted uncertainties are statistical only, with estimates of systematic errors discussed throughout the text of the paper and summarized in Table III. The curves shown in the figure include results of a fit to a Legendre-polynomial expansion and predictions of various partial-wave analyses.

The trend of our data is to be positive over the entire angular range and to increase with momentum in the forward direction. A comparison can be made with the published results of Albrow *et al.*,[5] which contained polarization parameters at 870, 910, and 970 MeV/$c$. Their results at 910 MeV/$c$ are statistically consistent with our 940-MeV/$c$ data but are systematically larger by a scale factor of approximately 1.1, while their data at 970 MeV/$c$ are systematically larger than our 940-MeV/$c$ results by a scale factor of approximately 1.23. As noted above, the trend in our data is for the polarization parameter to increase in the forward direction with increasing momentum. Thus, the lack of agreement between our data at 940 MeV/$c$ and the data at 970 MeV/$c$ may be due to changes in $P$ with momentum.

The 870-MeV/$c$ data of Ref. 5 are also systematically larger than our results at 940 MeV/$c$ and larger still than our results at 845 MeV/$c$. The inconsistencies between these data are more disturbing than those at the higher momenta since the large 870-MeV/$c$ polarizations are contrary to the trend of increasing polarization with momentum. While the disagreements between the higher-momentum points may be due to a systematic error in either of the experiments' measurement of the absolute value of target polarization, a systematic uncertainty of 6% for Ref. 5 and 5% for this experiment, such an error would not explain the difference in the trend of the data at the 870-MeV/$c$ point.

We have parametrized our results by the usual expansion in associated Legendre polynomials:

$$P\, d\sigma/d\Omega(\cos\theta_{\text{c.m.}}) = (1/k^2)\sum_{n=1}^{n_{\max}} B_n P_n^1(\cos\theta_{\text{c.m.}}), \qquad (5)$$

where $k$ is the center-of-mass wave number, $P_n^1$ are first associated Legendre polynomials of order $n$, and the $B_n$ are the coefficients to be determined. The differential cross sections employed in the fit were extracted from the literature[3-5] and parametrized in Legendre-polynomial expansions of the form

$$\frac{d\sigma}{d\Omega}(\cos\theta_{\text{c.m.}}) = \frac{1}{k^2}\sum_{n=0}^{n} A_n P_n(\cos\theta_{\text{c.m.}}). \qquad (6)$$

The value of $A_0$ was determined from published values of total cross sections.[1] At momenta where cross sections were unavailable, interpolations were made from nearby points. This is a valid procedure since the relevant cross sections vary slowly with beam momentum and interpolation was only necessary over 25 MeV/$c$. The resulting parameters for both the fits to the cross sections and our polarization data are given in Table IV.

Figure 5 displays our data along with several curves resulting from various analyses. Curves labeled A are derived from our Legendre-polynomial fit discussed above. Curves labeled B are results of an energy-dependent partial-wave analysis of Ref. 4. This analysis and its prediction of the polarization is typical of other analyses.[5,7] It used published cross sections at momenta between 150 and 1500 MeV/$c$, and polarization parameters between 870 and 1460 MeV/$c$. The curves, published before our results were available, are thus predictions of our data. The parametrization yields fits which are qualitatively in agreement with our measurements but predicts systematically larger polarizations than our results. This is most likely due to the 870-MeV/$c$ data of Ref. 5 employed in the fit and discussed previously in this paper. This class of solution has a $P_{13}$ partial-wave amplitude that exhibits a counterclockwise trajectory on an Argand diagram. Its speed, however, does not vary in the manner of a reso-

TABLE III. Summary of systematic errors.

| Nature of error | Estimated error |
|---|---|
| 1. Beam normalization and time variation of detector efficiency | ±0.03 [a] |
| 2. Target polarization | ±0.05 [b] |

[a] Adds linearly to polarization results.
[b] Multiplies scale of polarization.

TABLE IV. Legendre-polynomial coefficients. Cross sections are expanded as $d\sigma/d\Omega(\cos\theta_{\text{c.m.}}) = (1/k^2) \times\sum_n A_n P_n(\cos\theta_{\text{c.m.}})$, and $P\, d\sigma/d\Omega(\cos\theta_{\text{c.m.}}) = (1/k^2) \times\sum_n B_n P_n^1(\cos\theta_{\text{c.m.}})$, where $d\sigma/d\Omega$ is in mb/sr, and $k$ is in MeV/$c$.

| Momentum (MeV/$c$) | $A_0$ | $A_1$ | $A_2$ |
|---|---|---|---|
| 650 | 3.51 ± 0.06 | 0.07 ± 0.11 | 0.72 ± 0.14 |
| 700 | 2.92 ± 0.06 | 0.06 ± 0.12 | 0.99 ± 0.16 |
| 845 | 5.75 ± 0.09 | 0.00 ± 0.16 | 1.76 ± 0.22 |
| 940 | 7.55 ± 0.10 | 1.50 ± 0.20 | 2.57 ± 0.25 |
| **Momentum (MeV/$c$)** | **$B_1$** | **$B_2$** | **$B_3$** |
| 650 | 0.363 ± 0.026 | 0.038 ± 0.021 | 0.050 ± 0.022 |
| 700 | 0.340 ± 0.019 | 0.040 ± 0.015 | 0.027 ± 0.016 |
| 845 | 0.458 ± 0.018 | 0.093 ± 0.013 | 0.050 ± 0.015 |
| 940 | 0.605 ± 0.021 | 0.202 ± 0.016 | 0.073 ± 0.017 |

nance.

Curves C and D in Fig. 5 are results of a $K$-matrix analysis from which several $Z^*$ resonances have arisen.[8,9] A major difference between the generation of the two curves is that C was derived without our data as input while D included preliminary results of our polarization measurements. The results depicted in the former are in definite disagreement with our data at our two lower momenta while those in the latter are consistent with it. The $Z^*$ state emanating from these analyses, a $P_{13}$ pole initially reported at $(1787 - i\,100)$ MeV,[8] was unaffected by the reparametrization in fitting our results except for being shifted to $(1796 - i\,101)$ MeV.[9] This $K$-matrix analysis makes the strongest positive statement on the existence of $Z^*$ states of any currently published parametrizations. It is apparent, however, that its capability for prediction of new results is limited.

An interesting prediction of the polarization is seen in curve E.[12] This is the result of an analysis based on duality diagrams using the background amplitudes from $\pi^+p$ scattering as input data. The predictions using amplitudes referred to in Ref. 12 as the Almehed-Lovelace solution are pictured[13]; those of the Saclay solution[14] predicted polarizations that were too small for $\cos\theta_{\text{c.m.}}$ greater than zero for the 650 and 700 MeV/$c$ points, but adequately represented the data at 845 and 940 MeV/$c$. Since the model assumes that the background amplitudes in $\pi^+p$ and $K^+p$ scattering are the same and employs only the $\pi^+p$ background in predicting $K^+p$ data, it inherently has no resonant states in the $K^+p$ channel.

In summary, our measurements of the polarization parameters for $K^+p$ elastic scattering in the low-energy region are consistent with predictions which do not require resonant $Z^*$ states. Inasmuch as the analysis of Arndt *et al.*[9] can successfully fit our results, the question of the existence of these exotic states remains unresolved. The lack of anticipation of our results by the $K$-matrix approach, however, puts the reliability of the energy dependence of the amplitudes resulting from this analysis in doubt.

## ACKNOWLEDGMENTS

We gratefully acknowledge the contributions of L. Trudell for manufacturing the proportional chambers and scintillation counters, A. Etkin for building the polarized proton target, T. F. Kycia for loaning us the beam Cherenkov counter, and our colleagues, R. D. Ehrich and P. A. Souder, for their contributions to the experiment. We thank J. O. Dickey for useful discussions on the duality model and the technical staff and management of the AGS for their support and help during the construction and running of the experiment. This work was supported by the U. S. Department of Energy under Contract Nos. DE-AC02-76ER03075 and DE-AC02-76CH00016.

## APPENDIX

In this appendix we describe the procedure for comparing each event with the elastic-scattering hypothesis. The observed angle of a trajectory with respect to the incident beam direction at a particular detector was labeled $\eta_j$, where $j$ is the index of the appropriate detector: $j=1$ for $\theta_L$, $j=2$ for $\theta_R$, $j=3$ for $W\theta_L$, and $j=4$ for $W\theta_R$. For elastic scattering, observation of one point on the kaon or proton trajectory specifies the remaining points on both trajectories, and in our case, we chose to construct tables of calculated hit points based on the observed $\theta_L$ counter participating in the event. These tables assumed that the kaon or proton passed through the center of the $\theta_L$ counter on the median plane of the apparatus for the $K^+$-left and $K^+$-right hypotheses, respectively, and that the beam particle was incident along the axis of the beam line. Tables of derivatives of the trajectory angles with respect to variations of beam position, actual intersection of the kaon trajectory with the $\theta_L$ counter, and height of the kaon trajectory at $\theta_L$ were also constructed, as well as tables of center-of-mass scattering angles with appropriate derivatives and calculated errors on the $\eta_j$'s. These calculated errors included the effects of the resolution of the detector, multiple scattering in the target and uncertainty in the position of the interaction point in the target.

To summarize, labeling table values with a superscript $T$, we constructed tables of the following quantities:

$$\eta_j^T,\ \partial\eta_j^T/\partial x_B,\ \partial\eta_j^T/\eta z_B,\ \eta_j^T/\partial\theta_B,\ \partial\eta_j^T/\partial h\,,$$
$$\cos\theta^T_{\text{c.m.}},\ \partial(\cos\theta^T_{\text{c.m.}})/\partial\theta_K,\ \sigma_j^T\,;$$

where $x_B$ is the horizontal beam position with respect to the optic axis, $z_B$ is the longitudinal beam position as measured from the center of the target, $\theta_K$ is the deviation from the nominal table value of the laboratory angle of the scattered kaon, $h$ is the height of the kaon trajectory in the appropriate $\phi$ counter, and $\sigma_j^T$ is the calculated error on $\eta_j$.

The table values $\eta_j^T$, were corrected for nonzero $x_B$ and $h$ measured by the beam proportional chambers and $\phi$ counters, respectively, i.e.,

$$\eta_j^{T'} = \eta_j^T + \frac{\partial\eta_j^T}{\partial x_B}\,x_B + \frac{\partial\eta_j^T}{\partial h}\,h\,.$$

We then minimized the function:

$$\chi^2 = \sum_{j=1}^{4} \left[ \eta_j - \left( \eta_j^{T'} + \sum_{i=1}^{2} \delta x_i \frac{\partial \eta_j^T}{\partial x_i} \right) \right]^2 \Big/ \sigma_j^{T^2} ,$$

where $x_1 = z_B$ and $x_2 = \theta_K$, and $\delta x_i$ are the parameters with respect to which the $\chi^2$ function was minimized. The function $\sum \delta x_i \, \partial \eta_j^T / \partial x_i$ represents a correction to the variables $\eta_j^{T'}$ due to the fact that the interaction point was not necessarily in the longitudinal center of the target and that the left scattered particle did not necessarily pass through the center of the appropriate $\theta_L$ counter. The values $\delta x_i$ are then the deviations of the appropriate variables.

The minimized $\chi^2$ and the estimator of the coplanarity described in the main body of this paper are used to characterize the event as being signal or background. The corrected $\cos\theta^T_{\text{c.m.}}$ is then the assigned value of the cosine of the scattering angle for the event.

---

*Present address: Grumman Aerospace Corporation, Bethpage, N.Y.
†Present address: National Laboratory for High Energy Physics, KEK, Ibaraki, Japan.
‡Present address: Institute of Physics, University of Tsukuba, Ibaraki 305, Japan.

[1]R. L. Cool, G. Giacomelli, T. F. Kycia, B. A. Leontic, K. K. Li, A. Lundby, and J. Teiger, Phys. Rev. Lett. 17, 102 (1966); D. V. Bugg *et al.*, Phys. Rev. 168, 1466 (1968); T. Bowen, P. K. Caldwell, F. Ned Dikmen, E. W. Jenkins, R. M. Kalbach, D. V. Petersch, and A. E. Pifer, Phys. Rev. D 2, 2599 (1970); T. Bowen, E. W. Jenkins, R. M. Kalbach, D. V. Petersen, A. E. Pifer, and P. K. Caldwell, *ibid.* 7, 22 (1973); A. S. Carroll, T. F. Kycia, K. K. Li, D. N. Michael, P. M. Mockett, D. C. Rahm, and R. Rubinstein, Phys. Lett. 45B, 531 (1973).
[2]M. Gell-Mann, Phys. Lett. 8, 214 (1964).
[3]B. J. Charles *et al.*, Phys. Lett. 40B, 289 (1972); W. Cameron *et al.*, Nucl. Phys. B78, 93 (1974); R. A. Burnstein *et al.*, Phys. Rev. D 10, 2767 (1974); K. Abe *et al.*, *ibid.* 11, 1719 (1975).
[4]C. J. Adams *et al.*, Nucl. Phys. B66, 36 (1973).
[5]M. G. Albrow *et al.*, Nucl. Phys. B30, 273 (1971).
[6]R. D. Ehrlich *et al.*, Phys. Rev. Lett. 26, 925 (1971); B. A. Barnett *et al.*, Phys. Rev. D 8, 2751 (1973); R. Patton *et al.*, Phys. Rev. Lett. 34, 975 (1975).
[7]G. Giacomelli *et al.*, Nucl. Phys. B71, 138 (1974); B. R. Martin, *ibid.* B94, 413 (1975); R. E. Cutkosky *et al.*, *ibid.* B102, 139 (1976).
[8]R. A. Arndt, R. H. Hackman, L. D. Roper, and P. H. Steinberg, Phys. Rev. Lett. 33, 987 (1974).
[9]R. A. Arndt, L. D. Roper, and P. H. Steinberg, Phys. Rev. D 18, 3278 (1978).
[10]R. D. Ehrlich *et al.*, Phys. Lett. 71B, 455 (1977).
[11]Helv. Phys. Acta Suppl. 6, 436 (1961).
[12]J. O. Dickey, Nucl. Phys. B90, 501 (1975).
[13]S. Almehed and C. Lovelace, Nucl. Phys. B40, 157 (1972).
[14]A. Ayed and P. Bareyre, private communication.